**Climate
of the Past**

Open Access

Discussions

Diminished greenhouse warming from Archean methane due to solar absorption lines

B. Byrne and C. Goldblatt

School of Earth and Ocean Sciences, University of Victoria, Victoria, BC, Canada

CPD

10, 4229–4256, 2014

Archean radiative forcings

B. Byrne and C. Goldblatt

Title Page

Abstract	Introduction
Conclusions	References
Tables	Figures

|◄ | ►|
◄ | ►

Back | Close

Full Screen / Esc

Printer-friendly Version

Interactive Discussion

Abstract

Previous research has shown that methane may have been sustained at high concentrations in the Archean atmosphere, helping to offset lower insolation and solve the faint young sun problem. How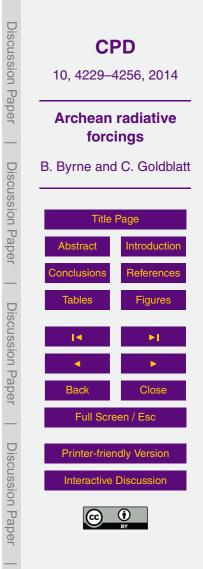ever, recent updates to the HITRAN line database have significantly increased the shortwave absorption by CH_4 in comparison to older versions of the database (e.g., HITRAN 2000). Here we investigate the climatological implications of strong shortwave CH_4 absorption in an Archean atmosphere rich in CH_4. We show that the surface warming at CH_4 abundances $> 10^{-3}$ is greatly diminished relative to the HITRAN 2000 line data. Strong shortwave absorption also results in a warm stratosphere and lower tropopause. We discuss these results in the context of contemporary research of the Archean climate and how these results could affect the formation of stratospheric clouds and an organic haze.

1 Introduction

The luminosity of the sun has increased steadily over its main sequence lifetime (Gough, 1981) and was 75–82 % as luminous in the Archean Eon (3.8–2.5 Gyr BP) as today. Despite a dimmer sun, geologic evidence suggests surface temperatures were similar to today for much of this period (Donn et al., 1965; Sagan and Mullen, 1972). The apparent contradiction between reduced solar luminosity and warm surface temperatures is termed the faint young sun problem or paradox (FYSP). It is generally believed that the Earth was kept warm in the Archean primarily due to elevated greenhouse gas concentrations and thus a stronger greenhouse effect.

Methane (CH_4) has a long photochemical lifetime of 10^3 to 10^4 yr in low oxygen atmospheres (Zahnle, 1986). Given the long atmospheric lifetime, concentrations of ≈ 10 ppmv could have been sustained by impacts from space and geologic sources in the Archean (Kasting, 2005). Much higher concentrations may have been sustained by anaerobic ecosystems. Using a photochemical–ecosystem model, Kharecha et al.
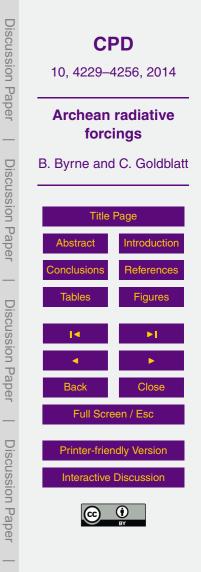
Full Screen / Esc

Printer-friendly Version

Interactive Discussion

(2005) found that biogenic methane fluxes were likely $1/3$ to 2.5 times modern values. They find that these fluxes could have sustained atmospheric concentrations of 100 to 35 000 ppmv (depending on the rate of hydrogen escape).

Thus, it has been proposed that methane played an important role in the Archean greenhouse and may have been partially responsible for the warm climate. At high CH_4/CO_2 ratios, photochemical reactions have been shown to produce an organic haze with a strong anti-greenhouse effect (Zahnle, 1986), possibly limiting the warming ability of CH_4 at very high concentrations.

Recent updates to the HITRAN database (Rothman et al., 2013; Brown et al., 2013) have significantly increased the magnitude of shortwave absorption by CH_4 at high concentration (Byrne and Goldblatt, 2014), particularly between 5500–9000 cm^{-1} and around 11 000 cm^{-1} (Fig. 1). This results in significant shortwave absorption in the upper troposphere and stratosphere at high CH_4 concentrations. It should be noted that there is still a considerable amount of missing shortwave line data, so the shortwave absorption by CH_4 is likely still being underestimated.

Strong shortwave absorption is expected to have a significant effect on the atmospheric temperature profile. Increased shortwave absorption in the stratosphere limits the amount of radiation that reaches the surface. As such, there is a negative forcing on the surface which acts to decrease surface temperatures. Thus, it is expected that previous estimates of the warming due to CH_4 have been over-estimated at high concentrations. Furthermore, solar absorption in the stratosphere leads to stratospheric warming, which diminishes the effect of greenhouse gases in the stratosphere.

In this paper, we run a radiative convective model (RCM) using the HITRAN 2000 and 2012 databases to examine the effect that updates to the HITRAN database have on the atmospheric profile and warming from CH_4. We choose the HITRAN 2000 version for comparison because most existing literature for CH_4 in the Archean uses shortwave absorption data which predates this version (Pavlov et al., 2000; Haqq-Misra et al., 2008). In Sect. 2, we describe our general methods. In Sect. 3, we provide our results. We examine the surface temperature and atmospheric profile as a function of CH_4.

In Sect. 4, we discuss the possible climatic consequences of our results. We discuss how a warmer stratosphere may affect stratospheric clouds and a hypothetical organic haze.
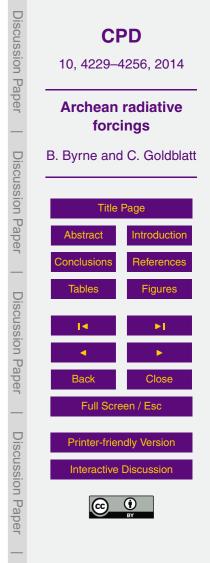
2 Methods

2.1 Radiative transfer model

We use the Spectral Mapping for Atmospheric Radiative Transfer (SMART) code, written by David Crisp (Meadows and Crisp, 1996), for our radiative transfer calculations. This code works at line-by-line resolution, but uses a spectral mapping algorithm to treat different wavenumber regions with similar optical properties together, giving significant savings in computational cost. We evaluate the radiative transfer in the range 50–100 000 cm^{-1} (0.1–200 μm) as a combined solar and thermal calculation. Line data for all radiatively active gases are taken from the HITRAN 2012 and 2000 databases.

2.2 Radiative Convective Model

The RCM used in this work derives from Goldblatt (2008) and Goldblatt et al. (2009). A "hard convective adjustment" is used, whereby the tropospheric structure is set as the moist adiabatic lapse rate, so surface and tropospheric temperature is represented by a single degree of freedom. The stratosphere is radiatively adjusted and the tropopause position is adjusted.

The SMART radiative transfer code is very computationally expensive. Hence the Newton–Raphson method used previously (Goldblatt et al., 2009) is too expensive, requiring a separate radiative transfer run for each degree of freedom (model level). Hence we derive a new numerical method which diagnoses a grey emissivity for each layer and solves a linearized set of equations to adjust the model temperature. The algorithm is described in full in the appendix. For test cases with a grey atmosphere

Archean radiative forcings
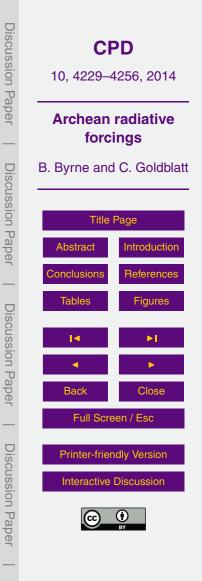
B. Byrne and C. Goldblatt

radiative transfer code, this gave convergence in 3–4 iterations. Unfortunately, the diagnosis of pseudo-grey emissivities for each layer from the real-gas radiation field was not as effective as we hoped and introduced some numerical instabilities. We introduced numerical smoothing and damping at each iteration to control the instability. Convergence was typically obtained in 20–30 iterations.

Water vapour was parametrized as in Manabe and Wetherald (1967). Relative humidity (h) is given by,

$$h = h_\star \left(\frac{Q - 0.02}{1 - 0.02} \right), \tag{1}$$

where $h_\star = 0.77$, $Q = p/p_\star$, and $p_\star$ is surface pressure. When Q is smaller than 0.02, the relative humidity becomes negative, thus it is necessary to specify a minimum humidity distribution for small Q values. Manabe and Wetherald (1967) assign a minimum mixing ratio of water vapour to be 3×10^{-6} g g^{-1} of air. We take this as the minimum mixing ratio for a "mid H$_2$O" set of calculations. Since the saturation vapour pressure is proportional to temperature and we expect significant warming in the upper troposphere and stratosphere from shortwave absorption by CH$_4$, the relative humidity parametrization may significantly affect the amount of atmospheric H$_2$O. The H$_2$O concentrations would then effect the strength of the H$_2$O greenhouse. Furthermore, elevated high troposphere and stratospheric water vapour concentrations would increase the emission level to space from H$_2$O and thus would promote cooling of this level. A further complication is that methane oxidation is a significant stratospheric moisture source, and this would be enhanced with higher methane abundances.

To examine the sensitivity of our results to the parametrization of H$_2$O we perform a "low H$_2$O" set of calculations for which we reduce the minimum mixing ratio of water vapour by a factor of 1000 to 3×10^{-9} g g^{-1} of air and a "high H$_2$O" set of calculations for which we increase the minimum mixing ratio of water vapour by a factor of 10 to 3×10^{-5} g g^{-1} of air. We attempted an additional set of runs where the H$_2$O mixing ratio

above the tropopause was set at the tropopause value but found it to be unstable with our model.

2.3 Runs

Gas amounts are given in abundances, a, relative to the modern atmosphere (1 bar, molecular weight of $28.97\,\text{g moles}^{-1}$, total moles ($n_0$) of $\approx 1.8 \times 10^{20}$). Thus $a = n_{\text{gas}}/n_0$. For our experiments we add gas abundances to background N_2 partial pressure (0.8 bar), increasing the atmospheric pressure.
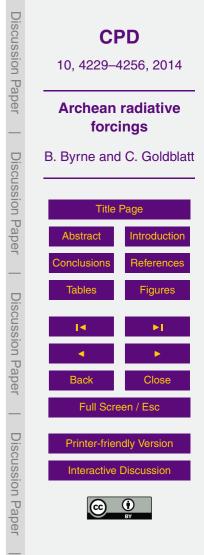
We calculate the equilibrium temperature profile over many CH_4 abundances in the range of 10^{-6} to 10^{-2} with a solar constant of 0.8 S_0. We perform sets of runs with background CO_2 abundances of 10^{-3}, 10^{-2}, and 10^{-1} for the "high H_2O", "mid H_2O" and "low H_2O" water vapour parametrizations. These sets of runs are performed with both the HITRAN 2000 and HITRAN 2012 line data, giving a total of 18 sets of runs. The reason for running sets with varying CO_2 abundances is that CO_2 cools the upper atmosphere and thus we would like to examine whether cooling by CO_2 or warming by CH_4 dominates.

3 Results

3.1 Modern atmosphere and climate sensitivity

To test our RCM and diagnose the climate sensitivity, we calculate the equilibrium temperature profile with pre-industrial (280 ppmv) and doubled (560 ppmv) CO_2. We find that our model performs well in recreating the pre-industrial atmospheric profiles (Fig. 2). For "low H_2O", "mid H_2O" and "high H_2O" parametrizations we find the pre-industrial surface temperature to be 288.4, 288.5, and 291.4 K. The temperature change for a doubling of CO_2 is 1.76 K for "low H_2O", 1.75 K for "mid H_2O" and 1.73 K for "high H_2O". These are within the range of climate sensitivities given by IPCC (2013)

(1.5–4.5 K) but are less than the best guess of 3 K. The climate sensitivity is largest for the "low H_2O" parametrization because the water vapour change is larger.
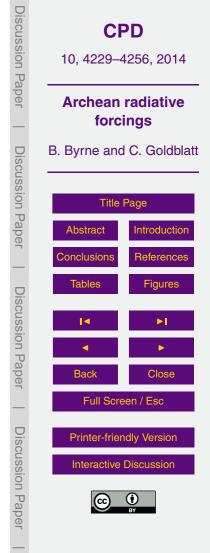
3.2 Error estimates

We take the model to be converged when the net flux above the tropopause (ΔF) is less than $0.2\,W\,m^{-2}$ for every layer above the tropopause. In cases where this could not be achieved within reasonable limits on computational cost, we estimate the precision of runs with a lower convergence threshold.

To do this we examined the difference in temperature for unconverged iterations of a converged run. The error in surface temperature for each unconverged iteration was found by taking the difference in surface temperature between the converged and unconverged iterations (ΔT). The maximum net flux above the tropopause was plotted as a function of surface temperature error (Fig. 3). To estimate the largest surface temperature error for a given maximum net flux above the tropopause we found a linear slope which contained all of the points. All of the points fit within a region bounded by a slope of $\Delta F = 2\Delta T$. Thus, uncertainty in temperature is taken to be $\Delta T = \frac{1}{2}\Delta F$.

3.3 Surface temperature

We examine surface temperature as a function of CH_4 for each set of runs (Fig. 4). For all cases, there are significant differences between runs with HITRAN 2000 and HITRAN 2012 line data. At low CH_4 abundances, the surface temperature is slightly warmer (≈ 1 K) using the HITRAN 2012 database relative to the HITRAN 2000 database due to additional longwave absorption lines added to the HITRAN 2012 database. Additional CH_4 shortwave absorption in HITRAN 2012 starts become evident at CH_4 above 10^{-4} and becomes significant at concentrations above 10^{-3}. For a CH_4 increase from 10^{-3} to 10^{-2} the warming is 4.8–6.4 K using HITRAN 2000 line data and −0.6–2.5 K using 2012 line data. Thus, the ability of CH_4 to warm the surface is significantly diminished above 10^{-3}.

Full Screen / Esc
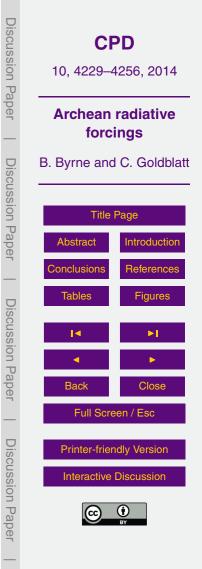
Printer-friendly Version

Interactive Discussion

The surface temperature is sensitive to the H_2O parametrization used. At low CH_4 abundances, the atmosphere is cold and the H_2O abundances decrease rapidly with altitude to the minimum allowed abundance (Fig. 5), resulting in large differences in the amount of atmospheric H_2O between the difference parametrizations. Thus, the water vapour greenhouse effect is much stronger for higher minimum allowed abundances, which results in warmer surface temperatures.

Large atmospheric methane abundances cause atmospheric warming above a pressure level of $0.3p_\star$ (see Sect. 3.4). For our low and mid H_2O parametrizations, this causes the amount of water here to increase, strengthening the greenhouse effect and causing surface warming. However, for our high H_2O parametrization, the water vapour is already at a maximum here and we see the consequence of methane absorption in isolation. between methane abundances of 3×10^{-4} and 1×10^{-2}, this is a surface cooling of 2 K with the HITRAN 2012 database as compared to a warming of 7 K using the HITRAN 2000 database.

The parametrizations of relative humidity used here are simplistic and may not properly represent the relative humidity structure for an Archean atmosphere with high CH_4. Water vapour moves from the troposphere to the stratosphere though complicated dynamical processes. On the modern Earth, water vapour enters the stratosphere through the extremely cold tropical tropopause (Brewer, 1949; Newell and Gould-Stewart, 1981). Resolving atmospheric dynamics would be required to correctly estimate stratospheric water vapour. Furthermore, methane oxidation is a significant source of stratospheric water vapour, and this will be a much larger source when there is more methane. Hence photochemistry should be treated too.

The surface temperatures calculated using HITRAN 2000 line data agrees well with the results of Haqq-Misra et al. (2008). For a CO_2 abundance of 10^{-2} and a CH_4 increase from 10^{-5} to 10^{-2}, Haqq-Misra et al. (2008) find a temperature increase of 11.5 K and we find a temperature increase of 12.6 K ("low H_2O"), 11.2 K ("mid H_2O") and 9.8 K ("high H_2O"). This is much diminished with the HITRAN 2012 line data, for

the same scenario we find a temperature increase of 8.1 K ("low H_2O"), 6.7 K ("mid H_2O") and 3.4 K ("high H_2O").

3.4 Atmospheric temperature structure

Increased shortwave absorption by CH_4 warms the stratosphere (altitudes above $\approx$ 0.3$p_\star$) relative to the HITRAN 2000 line data (Fig. 6). The warming as a function of CH_4 is roughly 2–5 K for 10^{-4}, 10–20 K for 10^{-3}, and 20–35 K for 10^{-2}. The warming also causes the tropopause to lower with increasing CH_4.

Elevated CO_2 acts to cool the stratosphere, and thus counteracts warming by CH_4. In general, warming by CH_4 is the dominant effect, although differences in the temperature structure at different CO_2 concentrations are apparent. The most significant differences are: (1) the difference in stratospheric temperature between the HITRAN databases is largest at low CO_2, (2) a temperature inversion appears for a CO_2 abundance of 10^{-3} but does not form at higher abundances, and (3) the tropopause is lower with less CO_2 (for example, with a CH_4 abundance of 10^{-2}, the tropopause is at $\approx 0.4p_\star$ for 10^{-3} of CO_2, $\approx 0.3p_\star$ for 10^{-2} of CO_2, and $\approx 0.2p_\star$ for 10^{-1} of CO_2).

Longwave emissions to space from H_2O act to cool the stratosphere. At low CH_4, higher parametrized H_2O abundances result in a cooler stratosphere. In contrast to the surface temperature, the H_2O parametrization has only a minor effect on the temperature structure in the stratosphere at high CH_4 concentrations. This is because the H_2O concentration is similar for all cases at high CH_4 (Fig. 5).

4 Discussion

4.1 Stratospheric ice clouds

In the contemporary modelling of the Archean atmosphere, the removal of O_2 and O_3 and increased CO_2 result in decreased static stability of the stratosphere (Rossow
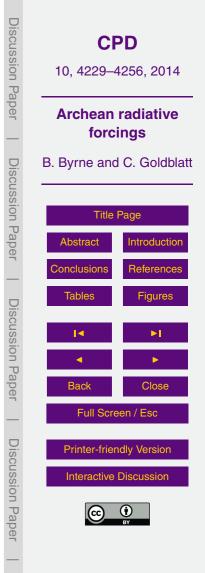
et al., 1982; Wolf and Toon, 2013; Kunze et al., 2014). Thus, deep convective mass and water fluxes are enhanced for the Archean (Wolf and Toon, 2013). However, as shown above, high CH_4 results in a stable stratosphere. Thus, it is worth discussing the effect that this increased stability would have on studies of the Archean climate.

Modelling studies have found that the removal of O_2 and O_3 results in a decrease in static stability and higher penetration of convection which produces increased cirrus ice clouds in the stratosphere (Rossow et al., 1982; Wolf and Toon, 2013; Kunze et al., 2014). Wolf and Toon (2013) find replacing O_2 and O_3 with N_2 in the present day atmosphere produces a $3.9\,W\,m^{-2}$ longwave radiative forcing from clouds. However, contribution of ice clouds to greenhouse effect in Archean is reduced due to the saturation of longwave spectral bands from elevated CO_2 concentrations despite increased cloud fractions. Thus, it is unlikely that the absence of these clouds would have a large effect on the Archean climate.

4.2 Organic haze

Photochemical models have found that an organic haze is produced by photolysis as CH_4 concentrations approach the CO_2 concentration in a low O_2 atmosphere (Kasting et al., 1983; Zahnle, 1986). Organic haze has been predicted by photochemical modelling at CH_4/CO_2 ratios larger than 1 (Zahnle, 1986), and laboratory experiments have found that organic haze could form at CH_4/CO_2 ratios as low as 0.2–0.3 (Trainer et al., 2004, 2006). The organic haze would likely produce a significant anti-greenhouse effect by reflecting solar radiation while being transparent to infrared radiation. Although the organic haze may also have shielded greenhouse gases from photolysis (such as NH_3 Wolf and Toon, 2010) and produced other greenhouse gases (such as C_2H_6, Haqq-Misra et al., 2008).

The precise radiative effect that an organic haze would have had on the early Earth's climate is poorly quantified. Further, the relative humidity at which the haze formed may have effected the radiative impacts of the haze. Hasenkopf et al. (2011) perform laboratory experiments on the formation of haze particles via ultraviolet photolysis over
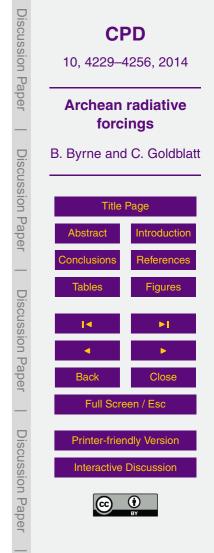
a range of relative humidities and find that increasing relative humidity increases the cooling effect of the haze particles. In contemporary Archean climate simulations, exceedingly low temperatures above the tropopause mean that saturation vapour pressure is quite low. Thus, despite having little water vapour, relative humidities grow large above the tropopause (Wolf and Toon, 2013). However, stratospheric warming would increase the saturation vapour pressure and lower the relative humidities which would effect the formation of an organic haze.

5 Conclusions

Increased shortwave absorption by CH_4 between the HITRAN 2000 and HITRAN 2012 databases significantly reduce the efficacy of CH_4 at warming the climate at abundances above 10^{-3}. The quantitative difference in warming is sensitive to the parametrization of relative humidity and the magnitude of water vapour change in our model. If the water vapour change is small ("high H_2O") then the surface temperature remains roughly constant or decreases with increasing CH_4 above an abundance of 10^{-3}. With a large H_2O change the surface temperature continues to increase with CH_4, but to a much lesser extent. These results are sensitive to our simple relative humidity parametrization; a GCM study with well resolved cross-tropospheric moisture transport and a parametrized moisture source from methane oxidation might be enlightening.

Significantly enhanced solar absorption here derives from the inclusion of the $11\,000\,cm^{-1}$ methane band in HITRAN 2012. However, there are still significant regions on missing data, especially around the $10\,000\,cm^{-1}$ (1 µm) methane band. Thus, we expect that our results here actually underestimate the true amount of absorption of sunlight by methane: surface cooling, stratospheric warming and tropopause lowering may all be larger than our calculations indicate.

The increased shortwave absorption significantly increases the stratospheric temperature and lowers the tropopause at high CH_4 concentrations. All relative humid-

ity parametrizations give high stratospheric H_2O at high CH_4 abundances and similar temperature structures. The warm temperature structure would reduce the likelihood of stratospheric ice clouds which have formed in some GCM studies of the Archean climate. They would also change the relative humidity of the stratosphere from those values seen in GCMs. Since the radiative properties of an organic haze is sensitive to the relative humidity at which it forms, this may significantly effect the radiative properties of such a haze.
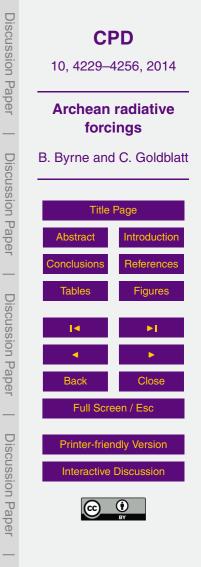
Appendix A: Radiative adjustment algorithm

The energy budget of an atmospheric layer is balanced by absorbed shortwave radiation, absorbed upwelling (D^+) and downwelling (D^-) longwave radiation, and emitted upwelling (B^+) and downwelling (B^-) longwave radiation.

The longwave radiation emitted at each atmospheric level is very sensitive to temperature. For simplicity, we assume that the emission from a layer j is independent of frequency and emitted as blackbody radiation (i.e., grey gas),

$$F_j^+ = a_j^+ \sigma T_j^4, \ F_j^- = a_j^- \sigma T_j^4, \tag{A1}$$

where a_j is the absorptivity/emissivity of a layer and T_j is the temperature of layer j. Since gases are not grey, we have to diagnose a_j as a pseudo-absorptivity (see Sect. A1).

The atmospheric profile given as an input to SMART consists of N levels, resulting in an atmosphere with $N - 1$ atmospheric layers. A layer with index j is bounded above by level j and below by level $j + 1$. We can write the fluxes absorbed and emitted from

layer j as,

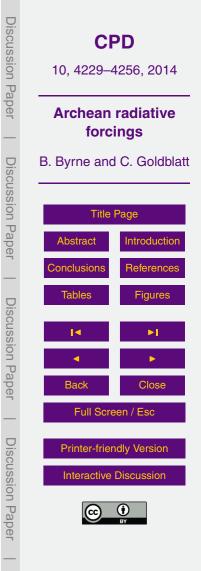$$D_j^-(T_1, \ldots, T_{j-2}, T_{j-1}) = \sigma a_j^- \sum_{n=1}^{j-1} \left[a_n^- T_n^4 \prod_{m=n+1}^{j-1} t_m^- \right],$$

$$D_j^+(T_{j+1}, T_{j+2}, \ldots, T_{\text{surf}}) = \sigma a_j^+ \left(\sum_{n=j+1}^{N-1} \left[a_n^+ T_n^4 \prod_{m=j+1}^{n-1} t_m^+ \right] + a_{\text{surf}}^+ T_{\text{surf}}^4 \prod_{m=j+1}^{N-1} t_m^+ \right),$$

$$B_j^-(T_j) = \sigma a_j^- \sigma T_j^4,$$

$$B_j^+(T_j) = \sigma a_j^+ \sigma T_j^4,$$

where $t_j = 1 - a_j$. So we have that the net absorbed flux (A_{net}) at layer j is,

$$A_{\text{net},j} = A_{\text{SW},j} + A_{\text{LW},j}, \tag{A2}$$

$$= A_{\text{SW},j} + D_j^- + D_j^+ - B_j^- - B_j^+. \tag{A3}$$

Let an initial atmospheric temperature profile have net absorbed radiation $A_{\text{net},j,0}$ and temperature $T_{j,0}$ for each layer j. Assume that there exists an equilibrium atmospheric temperature structure such that, $A_{\text{net},j} = 0$, for all j. The layer temperatures for the equilibrium profile, T_{E}, can then be written in terms of the initial layer temperatures and a temperature perturbation,

$$T_{\text{E},j} = T_{0,j} + \delta T_j. \tag{A4}$$

Full Screen / Esc

Printer-friendly Version

Interactive Discussion

The energy budget for the initial profile, for layer j, is given as

$$A_{\text{net},j,0} = A_{\text{SW},j} + D_j^-(T_{0,1}, \ldots, T_{0,j-2}, T_{0,j-1})$$
$$+ D_j^+(T_{0,j+1}, T_{0,j+2}, \ldots, T_{0,\text{surf}}) - B_j^-(T_{0,j}) - B_j^+(T_{0,j}),$$
$$= A_{\text{SW},j} + \sigma a_j^- \sum_{n=1}^{j-1} \left[a_n^- T_{0,n}^4 \prod_{m=n+1}^{j-1} t_m^- \right]$$
$$+ \sigma a_j^+ \left(\sum_{n=j+1}^{N-1} \left[a_n^+ T_{0,n}^4 \prod_{m=j+1}^{n-1} t_m^+ \right] + a_{\text{surf}}^+ T_{\text{surf}}^4 \prod_{m=j+1}^{N-1} t_m^+ \right)$$
$$- \sigma a_j^- \sigma T_{0,j}^4 - \sigma a_{0,j}^+ \sigma T_j^4, \tag{A5}$$

and the equilibrium profile (no net energy absorbed) is given,

$$0 = A_{\text{SW},j} + D_j^-(T_{0,1} + \delta T_1, \ldots, T_{0,j-2} + \delta T_{j-2}, T_{0,j-1} + \delta T_{j-1})$$
$$+ D_j^+(T_{0,j+1} + \delta T_{j+1}, T_{0,j+2} + \delta T_{j+2}, \ldots, T_{0,\text{surf}} + \delta T_{\text{surf}})$$
$$- B_j^-(T_{0,j} + \delta T_j) - B_j^+(T_{0,j} + \delta T_j).$$
$$= A_{\text{SW},j} + \sigma a_j^- \sum_{n=1}^{j-1} \left[a_n^-(T_{0,n} + \delta T_n)^4 \prod_{m=n+1}^{j-1} t_m^- \right]$$
$$+ \sigma a_j^+ \left(\sum_{n=j+1}^{N-1} \left[a_n^+(T_{0,n} + \delta T_n)^4 \prod_{m=j+1}^{n-1} t_m^+ \right] + a_{\text{surf}}^+(T_{\text{surf}} + \delta T_{\text{surf}})^4 \prod_{m=j+1}^{N-1} t_m^+ \right)$$
$$- \sigma a_j^- \sigma(T_{0,j} + \delta T_j)^4 - \sigma a_{0,j}^+ \sigma(T_{0,j} + \delta T_j)^4. \tag{A6}$$

Now, subtract Eq. (A6) from Eq. (A5),

$$A_{\text{net},j,0} = \sigma a_j^- \sum_{n=1}^{j-1} \left[a_n^- \left(T_{0,n}^4 - (T_{0,n} + \delta T_n)^4 \right) \prod_{m=n+1}^{j-1} t_m^- \right]$$

$$+ \sigma a_j^+ \left(\sum_{n=j+1}^{N-1} \left[a_n^+ \left(T_{0,n}^4 - (T_{0,n} + \delta T_n)^4 \right)^4 \prod_{m=j+1}^{n-1} t_m^+ \right] \right)$$

$$+ \sigma a_j^+ \left(a_{\text{surf}}^+ (T_{\text{surf}}^4 - (T_{\text{surf}} + \delta T_{\text{surf}})^4) \prod_{m=j+1}^{N-1} t_m^+ \right)$$

$$- \sigma a_j^- \sigma \left(T_{0,j}^4 - (T_{0,j} + \delta T_j)^4 \right) - \sigma a_{0,j}^+ \left(T_{0,j}^4 - (T_{0,j} + \delta T_j)^4 \right) \qquad \text{(A7)}$$

Expanding the terms results in numerous instances of $T_0^4 - (T_0 + \delta T)^4$. We can then approximate this as,

$$T_0^4 - (T_0 + \delta T)^4 = T_0^4 - \left(T_0^4 + 4T_0^3 \delta T + 6T_0^2 \delta T^2 + 4T_0^1 \delta T^3 + T_0^4 \right)$$

$$= -4T_0^3 \delta T - 6T_0^2 \delta T^2 - 4T_0^1 \delta T^3$$

$$= -4T_0^3 \delta T + O(\delta T^2),$$

$$\approx -4T_0^3 \delta T.$$

Archean radiative forcings

B. Byrne and C. Goldblatt

Back | Close

Full Screen / Esc

Printer-friendly Version

Interactive Discussion

Equation (

$$A_{\text{net},j,0} = \sigma a_j^- \sum_{n=1}^{j-1} \left[a_n^- \left(-4T_{0,n}^3 \delta T_n \right) \prod_{m=n+1}^{j-1} t_m^- \right]$$

$$+ \sigma a_j^+ \left(\sum_{n=j+1}^{N-1} \left[a_n^+ \left(-4T_{0,n}^3 \delta T_n \right) \prod_{m=j+1}^{n-1} t_m^+ \right] \right)$$

$$+ \sigma a_j^+ \left(a_{\text{surf}}^+ \left(-4T_{0,\text{surf}}^3 \delta T_{\text{surf}} \right) \prod_{m=j+1}^{N-1} t_m^+ \right)$$

$$- \sigma a_j^- \left(-4T_{0,j}^3 \delta T_j \right) - \sigma a_j^+ \left(-4T_{0,j}^3 \delta T_j \right)$$

$$= -4\sigma a_j^- \sum_{n=1}^{j-1} \left[a_n^- \left(T_{0,n}^3 \delta T_n \right) \prod_{m=n+1}^{j-1} t_m^- \right]$$

$$- 4\sigma a_j^+ \left(\sum_{n=j+1}^{N-1} \left[a_n^+ T_{0,n}^3 \delta T_n \prod_{m=j+1}^{n-1} t_m^+ \right] + a_{\text{surf}}^+ T_{0,\text{surf}}^3 \delta T_{\text{surf}} \prod_{m=j+1}^{N-1} t_m^+ \right)$$

$$+ 4\sigma \left(a_j^- T_{0,j}^3 \delta T_j + a_j^+ T_{0,j}^3 \delta T_j \right)$$

so,

$$\frac{1}{4\sigma} A_{\text{net},j,0} = -a_j^- \sum_{n=1}^{j-1} \left[a_n^- \left(T_{0,n}^3 \delta T_n \right) \prod_{m=n+1}^{j-1} t_m^- \right]$$

$$- a_j^+ \left(\sum_{n=j+1}^{N-1} \left[a_n^+ T_{0,n}^3 \delta T_n \prod_{m=j+1}^{n-1} t_m^+ \right] + a_{\text{surf}}^+ T_{0,\text{surf}}^3 \delta T_{\text{surf}} \prod_{m=j+1}^{N-1} t_m^+ \right)$$

$$+ \left(a_j^- T_{0,j}^3 \delta T_j + a_j^+ T_{0,j}^3 \delta T_j \right)$$

Consider this for every atmospheric layer. This system of linear equations can be written as:

$$\frac{1}{4\sigma}\mathbf{A_{net,0}} = \mathbf{\Lambda}\delta\mathbf{T}, \tag{A8}$$

where,

$$\mathbf{A_{net,0}} = \begin{bmatrix} A_{net,1,0} \\ A_{net,2,0} \\ \vdots \\ A_{net,N-1,0} \\ A_{net,N,0} \end{bmatrix},$$

$$\mathbf{\Lambda} = \begin{bmatrix} (a_1^+ + a_1^-)T_1^3 & -a_1^+ a_2^+ T_2^3 & \cdots & -a_1^+ a_{surf}^+ t_{j+1}^+ \cdots t_{N-1}^+ T_{surf}^3 \\ -a_2^- a_1^- T_1^3 & (a_2^+ + a_2^-)T_2^3 & \cdots & -a_2^+ a_{surf}^+ t_{j+1}^+ \cdots t_{N-1}^+ T_{surf}^3 \\ \vdots & \vdots & \ddots & \vdots \\ -a_{N-1}^- a_1^- t_2^- \cdots t_{N-1}^- T_1^3 & -a_{N-1}^- a_2^- t_3^- \cdots t_{N-1}^- T_2^3 & \cdots & a_{N-1}^+ a_{surf}^+ T_{surf}^3 \\ -a_{surf}^- a_1^- t_2^- \cdots t_j^- T_1^3 & -a_{surf}^- a_2^- t_3^- \cdots t_N^- T_2^3 & \cdots & a_{surf}^+ T_{surf}^3 \end{bmatrix},$$

and,

$$\delta\mathbf{T} = \begin{bmatrix} \delta T_1 \\ \delta T_2 \\ \vdots \\ \delta T_{N-1} \\ \delta T_N \end{bmatrix}.$$

Then Eq. (7) can be solved for $\delta\mathbf{T}$,

$$\delta\mathbf{T} = \frac{1}{4\sigma}\mathbf{\Lambda}^{-1}\mathbf{A_{net,0}}, \tag{A9}$$

which can be used to solve for the equilibrium temperature at each atmospheric layer and at the surface,

$$\mathbf{T_E} = \mathbf{T_0} + \delta\mathbf{T}. \tag{A10}$$

A1 Diagnosing absorptivity

The absorptivity is diagnosed as follows. We have that the absorbed radiation A_b for a layer j is given by,

$$A_b = F^+_{LW,j+1} - F^+_{LW,j},$$
$$= a^+_j F^+_{LW,j+1} - a^+_j \sigma T^4_j,$$

so that,

$$a^+_j \left(F^+_{LW,j+1} - \sigma T^4_j \right) = F^+_{LW,j+1} - F^+_{LW,j},$$
$$a^+_j = \frac{F^+_{LW,j+1} - F^+_{LW,j}}{F^+_{LW,j+1} - \sigma T^4_j},$$

and similarly,

$$a^-_j = \frac{F^-_{LW,j} - F^-_{LW,j+1}}{F^-_{LW,j} - \sigma T^4_j}.$$

The upward (a_+) and downward (a^-) absorption coefficients are different because the spectral intensities of radiation incident on the layer are different. The upward propagating longwave radiation's spectra is heavily influenced by the emission spectra of water vapour and the surface, whereas, the downward propagating radiation's spectra is mainly emanating from the well-mixed greenhouse gases.

Archean radiative forcings

B. Byrne and C. Goldblatt

Title Page

Abstract	Introduction
Conclusions	References
Tables	Figures

◄◄	►►
◄	►
Back	Close

Full Screen / Esc

Printer-friendly Version

Interactive Discussion

Discussion Paper | Discussion Paper | Discussion Paper | Discussion Paper |

CPD

10, 4229–4256, 2014

Archean radiative forcings

B. Byrne and C. Goldblatt

Title Page

Abstract | Introduction

Conclusions | References

Tables | Figures

|◄ | ►|

◄ | ►

Back | Close

Full Screen / Esc

Printer-friendly Version

Interactive Discussion

A2 Implementation of the algorithm

To implement the algorithm, the troposphere is taken to be a single level in the model. The tropopause temperature is taken to be the level temperature. The temperature adjustment for the level is scaled by a factor of 1/4 and applied at the surface. The pseudo-adiabatic lapse rate is followed from the adjusted surface up to the tropopause (if the tropopause is colder, the pseudo-adiabat is followed to the lowest level which exceeds the pseudo-adiabatic temperature profile).

However, this algorithm cannot lower the tropopause in a warming atmosphere. To account for this, we perform the algorithm again but treat the atmosphere from the surface to the layer below the tropopause as a single layer. The temperature adjustment is then only applied to the tropopause (if it is a warming).
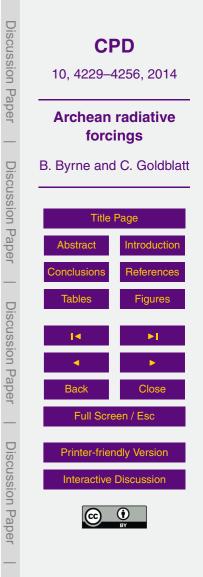
References

Brewer, A.: Evidence for a world circulation provided by the measurements of helium and water vapour distribution in the stratosphere, Q. J. Roy. Meteor. Soc., 75, 351–363, doi:10.1002/qj.49707532603, 1949. 4236
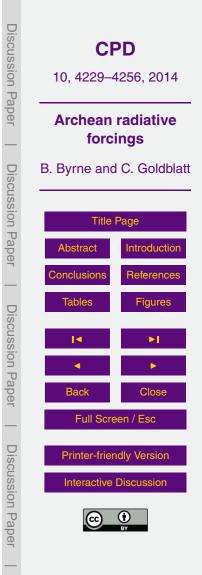
Brown, L. R., Sung, K., Benner, D. C., Devi, V. M., Boudon, V., Gabard, T., Wenger, C., Campargue, A., Leshchishina, O., Kassi, S., Mondelain, D., Wang, L., Daumont, L., Regalia, L., Rey, M., Thomas, X., Tyuterev, V. G., Lyulin, O. M., Nikitin, A. V., Niederer, H. M., Albert, S., Bauerecker, S., Quack, M., O'Brien, J. J., Gordon, I. E., Rothman, L. S., Sasada, H., Coustenis, A., Smith, M. A. H., Carrington Jr., T., Wang, X.-G., Mantz, A. W., and Spickler, P. T.: Methane line parameters in the HITRAN2012 database, J. Quant. Spectrosc. Ra., 130, 201–219, doi:10.1016/j.jqsrt.2013.06.020, 2013. 4231

Byrne, B. and Goldblatt, C.: Radiative forcing at high concentrations of well-mixed greenhouse gases, Geophys. Res. Lett., 41, 152–160, doi:10.1002/2013GL058456, 2014. 4231

Donn, W. L., Donn, B. D., and Valentine, W. G.: On the early history of the Earth, Geol. Soc. Am. Bull., 76, 287–306, doi:10.1130/0016-7606(1965)76[287:OTEHOT]2.0.CO;2, 1965. 4230

5 Goldblatt, C.: Bistability of atmospheric oxygen, the Great Oxidation and climate, Ph. D. thesis, Univ. East Anglia, 2008. 4232

Goldblatt, C., Claire, M. W., Lenton, T. M., Matthews, A. J., Watson, A. J., and Zahnle, K. J.: Nitrogen-enhanced greenhouse warming on early Earth, Nat. Geosci., 2, 891–896, doi:10.1038/NGEO692, 2009. 4232

10 Gough, D.: Solar interior structure and luminoscity variations, Sol. Phys., 74, 21–34, doi:10.1007/BF00151270, 1981. 4230

Haqq-Misra, J. D., Domagal-Goldman, S. D., Kasting, P. J., and Kasting, J. F.: A revised, hazy methane greenhouse for the archean earth, Astrobiology, 8, 1127–1137, doi:10.1089/ast.2007.0197, 2008. 4231, 4236, 4238

15 Hasenkopf, C. A., Freedman, M. A., Beaver, M. R., Toon, O. B., and Tolbert, M. A.: Potential climatic impact of organic haze on early earth, Astrobiology, 11, 135–149, doi:10.1089/ast.2010.0541, 2011. 4238

IPCC: Climate Change 2013: The Scientific Basis. Contribution of Working Group I to the Fifth Assessment Report of the Intergovernmental Panel on Climate Change, Cambridge University Press, Cambridge, UK, and New York, NY, USA, 2013. 4234

20 Kasting, J.: Methane and climate during the Precambrian era, Precambrian Res., 137, 119–129, doi:10.1016/j.precamres.2005.03.002, 2005. 4230

Kasting, J., Zahnle, K., and Walker, J.: Photochemistry of methane in the Earth's early atmosphere, Precambrian Res., 20, 121–148, doi:10.1016/0301-9268(83)90069-4, 1983. 4238

25 Kharecha, P., Kasting, J., and Siefert, J.: A coupled atmosphere-ecosystem model of the early Archean Earth, Geobiology, 3, 53–76, doi:10.1111/j.1472-4669.2005.00049.x, 2005. 4230

Kunze, M., Godolt, M., Langematz, U., Grenfell, J. L., Hamann-Reinus, A., and Rauer, H.: Investigating the early Earth faint young Sun problem with a general circulation model, Planet. Space Sci., 98, 77–92, doi:10.1016/j.pss.2013.09.011, 2014. 4238

30 Manabe, S. and Wetherald, R.: Thermal equilibrium of the atmosphere with a given distribution of relative humidity, J. Atmos. Sci., 24, 241–259, doi:10.1175/1520-0469(1967)024<0241:TEOTAW>2.0.CO;2, 1967. 4233

Title Page

Abstract | Introduction

Conclusions | References

Tables | Figures

◄ | ►

◄ | ►

Back | Close

Full Screen / Esc

Printer-friendly Version

Interactive Discussion

Meadows, V. and Crisp, D.: Ground-based near-infrared observations of the Venus nightside: the thermal structure and water abundance near the surface, J. Geophys. Res.-Planet, 101, 4595–4622, doi:10.1029/95JE03567, 1996. 4232

Newell, R. and Gould-Stewart, S.: A stratospheric fountain, J. Atmos. Sci., 38, 2789–2796, doi:10.1175/1520-0469(1981)038<2789:ASF>2.0.CO;2, 1981. 4236
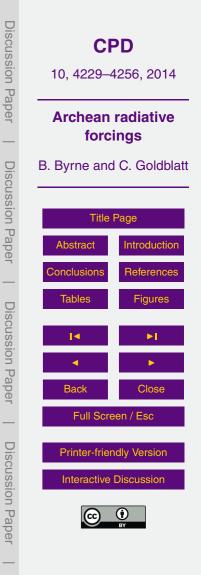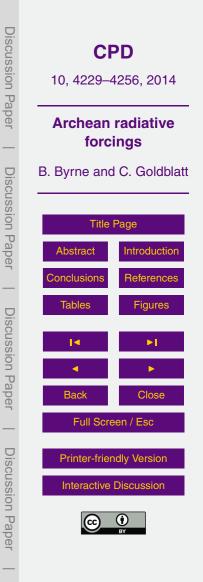
Pavlov, A., Kasting, J., Brown, L., Rages, K., and Freedman, R.: Greenhouse warming by CH_4 in the atmosphere of early Earth, J. Geophys. Res.-Planet, 105, 11981–11990, doi:10.1029/1999JE001134, 2000. 4231

Rossow, W., Henderson-Sellers, A., and Weinreich, S.: Cloud feedback – a stabilizing effect for the early Earth, Science, 217, 1245–1247, doi:10.1126/science.217.4566.1245, 1982. 4237, 4238

Rothman, L. S., Gordon, I. E., Babikov, Y., Barbe, A., Benner, D. C., Bernath, P. F., Birk, M., Bizzocchi, L., Boudon, V., Brown, L. R., Campargue, A., Chance, K., Cohen, E. A., Coudert, L. H., Devi, V. M., Drouin, B. J., Fayt, A., Flaud, J. M., Gamache, R. R., Harrison, J. J., Hartmann, J. M., Hill, C., Hodges, J. T., Jacquemart, D., Jolly, A., Lamouroux, J., Le Roy, R. J., Li, G., Long, D. A., Lyulin, O. M., Mackie, C. J., Massie, S. T., Mikhailenko, S., Mueller, H. S. P., Naumenko, O. V., Nikitin, A. V., Orphal, J., Perevalov, V., Perrin, A., Polovtseva, E. R., Richard, C., Smith, M. A. H., Starikova, E., Sung, K., Tashkun, S., Tennyson, J., Toon, G. C., Tyuterev, V. G., and Wagner, G.: The HITRAN2012 molecular spectroscopic database, J. Quant. Spectrosc. Ra., 130, 4–50, doi:10.1016/j.jqsrt.2013.07.002, 2013. 4231

Sagan, C. and Mullen, G.: Earth and Mars – evolution of atmospheres and surface temperatures, Science, 177, 52–56, doi:10.1126/Science.177.4043.52, 1972. 4230

Trainer, M., Pavlov, A., Curtis, D., McKay, C., Worsnop, D., Delia, A., Toohey, D., Toon, O., and Tolbert, M.: Haze aerosols in the atmosphere of early earth: manna from heaven, Astrobiology, 4, 409–419, doi:10.1089/ast.2004.4.409, 2004. 4238

Trainer, M. G., Pavlov, A. A., DeWitt, H. L., Jimenez, J. L., McKay, C. P., Toon, O. B., and Tolbert, M. A.: Organic haze on Titan and the early Earth, P. Natl. Acad. Sci. USA, 103, 18035–18042, doi:10.1073/pnas.0608561103, 2006. 4238
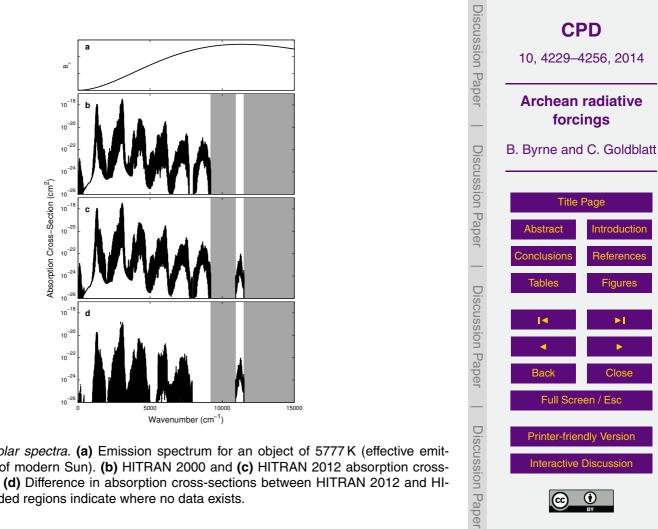
Wolf, E. T. and Toon, O. B.: Fractal organic hazes provided an ultraviolet shield for early Earth, Science, 328, 1266–1268, doi:10.1126/Science.1183260, 2010. 4238

Wolf, E. T. and Toon, O. B.: Hospitable archean climates simulated by a general circulation model, Astrobiology, 13, 656–673, doi:10.1089/ast.2012.0936, 2013. 4238, 4239

Title Page

Abstract | Introduction

Conclusions | References

Tables | Figures

◀ | ▶

◀ | ▶

Back | Close

Full Screen / Esc

Printer-friendly Version

Interactive Discussion

Zahnle, K.: Photochemistry of methane and the formation of hydrocyanic acid (HCN) in the earth's early atmosphere, J. Geophys. Res., 91, 2819–2834, doi:10.1029/JD091iD02p02819, 1986. 4230, 4231, 4238
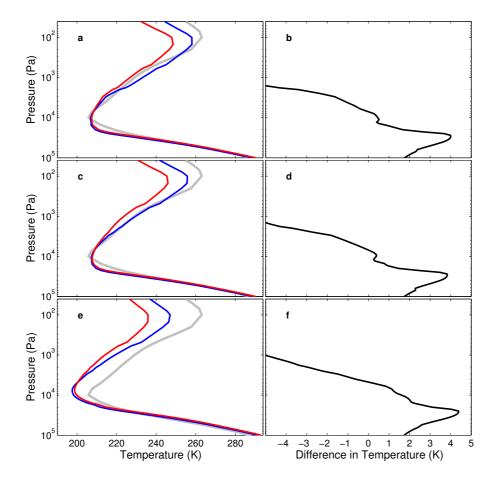
Figure 1. CH$_4$ *solar spectra*. **(a)** Emission spectrum for an object of 5777 K (effective emitting temperature of modern Sun). **(b)** HITRAN 2000 and **(c)** HITRAN 2012 absorption cross-sections for CH$_4$. **(d)** Difference in absorption cross-sections between HITRAN 2012 and HITRAN 2000. Shaded regions indicate where no data exists.
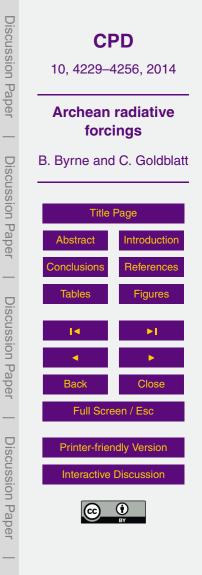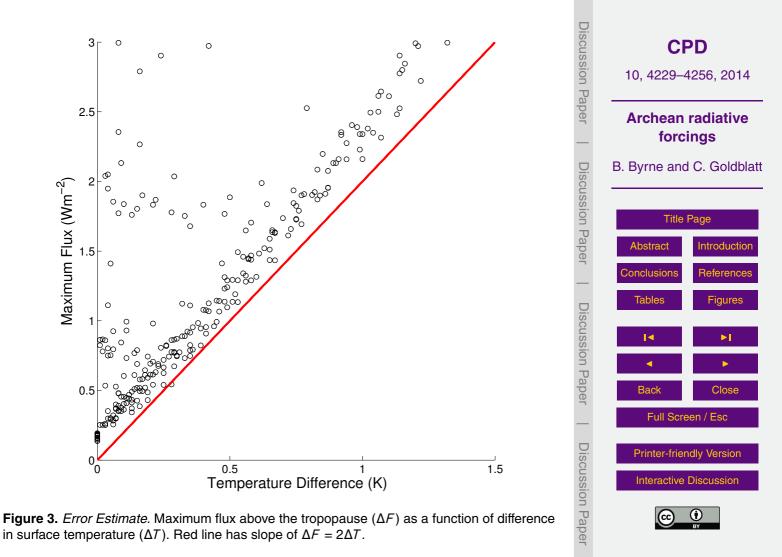
Figure 2. *Modern Earth temperature profiles.* Pre-industrial (blue) and doubled CO_2 (red) temperature profiles for **(a)** low, **(c)** mid, and **(e)** high H_2O parametrizations. Corresponding changes in temperature for **(b)** low, **(d)** mid, and **(f)** high H_2O parametrizations. Grey line shows the global and annual mean modern day temperature profile.
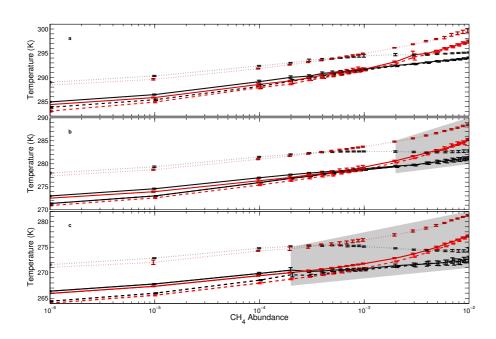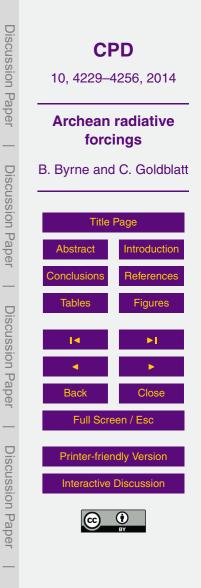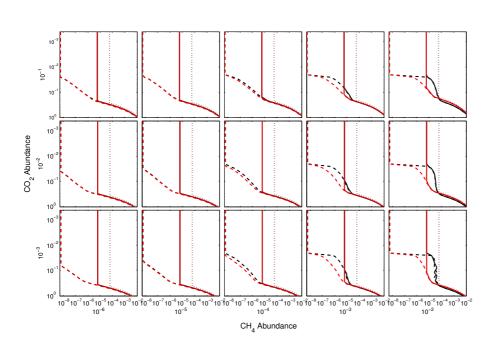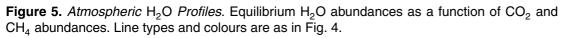
Figure 3. *Error Estimate.* Maximum flux above the tropopause (ΔF) as a function of difference in surface temperature (ΔT). Red line has slope of $\Delta F = 2\Delta T$.

Title Page

Abstract | Introduction

Conclusions | References

Tables | Figures

◄ | ►►

◄ | ►

Back | Close

Full Screen / Esc

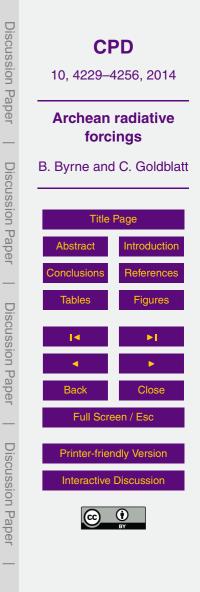Printer-friendly Version

Interactive Discussion

Figure 4. *Surface Temperature as a function of* CH_4. The three panels correspond to CO_2 abundances of **(a)** 10^{-1}, **(b)** 10^{-2}, and **(c)** 10^{-3}. Dashed lines are for the "low H_2O" parametrization, solid lines are for the "mid H_2O" parametrization and dotted lines are for the "high H_2O" parametrization. Black lines are for the HITRAN 2012 database and red lines are for the HITRAN 2000 database. Shaded regions indicate the possibility of an organic haze.
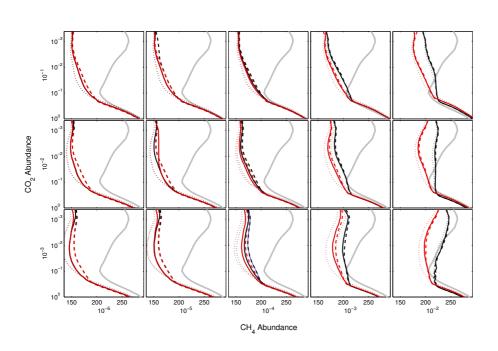
Figure 5. *Atmospheric* H_2O *Profiles*. Equilibrium H_2O abundances as a function of CO_2 and CH_4 abundances. Line types and colours are as in Fig. 4.

Figure 6. *Atmospheric Temperature Profiles.* Equilibrium temperature profiles (K) as functions of CO_2 and CH_4 abundances. Line types and colours are as in Fig. 4. Grey line shows the global and annual mean temperature profile for the modern atmosphere.